PCCP

PAPER

View Article Online
View Journal | View Issue

Cite this: *Phys. Chem. Chem. Phys.*, 2014, **16**, 2515

The use of ^{6}Li{^{7}Li}-REDOR NMR spectroscopy to compare the ionic conductivities of solid-state lithium ion electrolytes†

T. L. Spencer,[a] N. W. Plagos,[a] D. H. Brouwer[b] and G. R. Goward*[a]

Received 23rd September 2013,
Accepted 10th December 2013

DOI: 10.1039/c3cp55132f

www.rsc.org/pccp

Garnet-like solid-state electrolyte materials for lithium ion batteries are promising replacements for the currently-used liquid electrolytes. This work compares the temperature dependent Li^+ ion hopping rate in $Li_6BaLa_2M_2O_{12}$ (M = Ta, Nb) using solid-state ^{6}Li{^{7}Li}-REDOR NMR. The slope of the ^{6}Li{^{7}Li}-REDOR curve is highly temperature dependent in these two phases, and a comparison of the changes of the REDOR slopes as a function of temperature has been used to evaluate the Li^+ ion dynamics. Our results indicate that the Nb phase has a higher overall ionic conductivity in the range of 247 K to 350 K, as well as a higher activation energy for lithium ion hopping than the Ta counterpart. For appropriate relative timescales of the dipolar couplings and ion transport processes, this is shown to be a facile method to compare ion dynamics among similar structures.

1.0. Introduction

Lithium ion batteries (LIBs) provide light-weight energy storage for many portable electronic devices.[1,2] This technology is being groomed for extension into the automotive industry with applications in hybrid and electric vehicles. Automotive applications require batteries with lighter weight, higher energy density, and moreover, adherence to stringent safety requirements.[3–5] There has been a significant focus on novel cathode and anode materials for lithium ion batteries, with the aim of improving cycle life and charging rates.[2,3,6–13] Nevertheless, the currently used liquid electrolytes continue to place constraints on the output voltage of the battery, decomposing below 5 V, while posing significant fire-risk in traditional LIB cells.[3]

Solid-state ceramic lithium ion electrolytes are non-flammable and withstand a higher voltage window than traditional liquid or polymer electrolytes. Moreover, they show little reactivity with cathode and anode materials where traditional electrolyte materials are known to form a solid electrolyte interface (SEI), which may be unstable, and consume Li^+, shortening the lifetime of the battery.[3,14–17] For these reasons, solid-state lithium ion electrolytes provide a method of attaining the stability necessary for batteries to be used in the automotive industry. Within this class of materials, garnet-like ceramic electrolytes exhibit excellent lithium ion conductivity.[16,18–20] The garnet-like materials $Li_6BaLa_2M_2O_{12}$ (M = Ta, Nb) display among the highest ionic conductivities with the Ta phase having a reported conductivity of 4×10^{-5} S cm^{-1}.[21]

Structurally, garnet-like ceramic electrolytes resemble traditional garnets, consisting of an array of large tetrahedrally- and octahedrally-coordinated transition metal cations sharing oxygen corners.[18,22] Lithium ions also occupy octahedral and tetrahedral sites and there has been disagreement in the literature concerning the number of unique crystallographic lithium sites in this class of materials. Some authors claim that Li is distributed between a single octahedral site and a single tetrahedral site, while others report that there are two octahedral and one tetrahedral sites.[18,23,24] In addition, the exact occupancy of these sites is difficult to quantify, and may substantially impact the conductivity observed. This occupancy issue may be responsible for the differing conductivities observed by groups studying these phases.

Previous studies have made use of a combination of powder X-ray diffraction and electron density distribution methods to investigate garnet-like materials.[14–16,21,24–27] Results from some authors have shown that for the Ta phase the tetrahedral site, Li-1, is 30% occupied, while the octahedral site, Li-2, is 42% occupied. Note that the multiplicities for the Li-1 and Li-2 sites are 24 and 96, respectively, making the contribution from the Li-1 and Li-2 sites 15% and 85%, respectively indicating that there is substantially more lithium in the Li-2 site.[26] At this point similar studies have not yet been performed for the Nb phase, and thus there is no report in the literature of the lithium ion occupancy for this phase. However, efforts have

[a] *McMaster University, Department of Chemistry and Chemical Biology, 1280 Main St. West, Hamilton, Ontario, Canada, L8S 1H2. E-mail: goward@mcmaster.ca; Fax: +1-905-522-2509; Tel: +1-905-525-9140 x 24176*
[b] *Redeemer University College, Department of Chemistry, 777 Garner Road East, Ancaster, ON, Canada, L9K 1J4*

† Electronic supplementary information (ESI) available. See DOI: 10.1039/c3cp55132f

been made to understand the effect of overall lithium content on the ionic conductivity in garnet-like electrolyte materials and several studies have found that an increase in lithium content in the octahedral site can increase the ionic conductivity.[27,28]

Solid-state nuclear magnetic resonance (ssNMR) has been used in an attempt to assign the relative tetrahedral and octahedral sites.[27–29] In this work we use the assignment proposed by previous authors, in which the garnet-like material $Li_5La_3Nb_2O_{12}$ was studied using ^{6}Li and ^{7}Li MAS NMR spectroscopy. In this study a combination of ^{6}Li{^{7}Li}-Cross Polarization Magic Angle Spinning (^{6}Li{^{7}Li}-CPMAS) NMR and ^{6}Li{^{7}Li}-Cross Polarization MAS-Rotational Double Echo Resonance (^{6}Li-{^{7}Li}-CPMAS-REDOR) NMR was used to determine that of the two observed ^{7}Li spectral resonances the octahedral site was found at +0.7 ppm (^{6}Li NMR spectra), while the tetrahedral site was found at −0.2 ppm.[28]

In addition to the structural assignment of the ^{7}Li NMR spectral sites, it is important to determine which crystallographic site is responsible for ionic motion in this class of materials. Here, we use the assignment given by previous studies of the garnet structure $Li_{3+x}Nd_3Te_{2-x}Sb_xO_{12}$, in which solid-state ^{7}Li MAS NMR was used to determine that the tetrahedral lithium ions are held tightly in place, while the octahedral lithium ions are held more loosely and are therefore primarily responsible for the ionic motion in these systems. These results are based on the trend observed when the occupancy of the octahedral site was increased synthetically, which resulted in an increase in ionic conductivity of the material, measured using bulk impedance analysis. High temperature ssNMR studies were performed, which showed no coalescence between the two observed ^{7}Li resonances and therefore the authors concluded that there was no chemical exchange between the two lithium environments and that the octahedral site is responsible for ion motion. The authors noted a significant difference in the T_1 relaxation rates of the two ^{7}Li resonances. The tetrahedral site had a T_1 relaxation which consisted of two components, 15 s and 5 min; while the octahedral site had a T_1 with a single component of 8 ms.[27]

Koller and Kalwei have used the REDOR NMR spectroscopy experiments and second moment, M_2, analysis to consider rotational ion motion in tetrahydroxyborate sodalite. In their work several REDOR experiments were performed: ^{11}B{^{1}H}-REDOR, ^{27}Al{^{11}B}-REDOR and ^{23}Na{^{11}B}-REDOR. The study aimed to determine the nature of ion motion in a sodalite material using REDOR methods to probe re-orientation of anions and sodium motion. This work emphasized the limitation of 1D variable temperature line-narrowing studies for this system and instead made use of the temperature dependence of the observed REDOR curves in combination with M_2 calculations to evaluate the motion in the sodium system. In addition, the authors tackled the contribution of the quadrupole coupling, which is present for several nuclei in the system and can affect the REDOR experiment.[30]

The present work describes a similar method, which uses solid-state ^{6}Li{^{7}Li}-REDOR NMR spectroscopy to qualitatively characterize and compare the lithium ion mobility in the garnet-like structures $Li_6BaLa_2Ta_2O_{12}$ and $Li_6BaLa_2Nb_2O_{12}$.[16,26,31] This method can be used to study materials in which chemical exchange occurs between neighbouring lithium ions, which occupy the same site in the crystal structure. In such cases, the use of 2D exchange NMR is not straight-forward, particularly for nuclei which do not possess substantial chemical shielding anisotropy, such as lithium. It is expected that this method can be extended into systems that have previously not been studied using 2D EXSY NMR. The type of motion in this system is different from that studied by Koller *et al.*[30] in that Li ions in $Li_6BaLa_2M_2O_{12}$ (M = Ta, Nb) move *via* discreet jumps between neighbouring sites, and there is no corresponding anion rotation. The complexity of this motion makes modelling the dynamics in this system challenging.

Table 1 Comparing the Li ion conductivity and activation energy of Li ion hopping in $Li_6BaLa_2M_2O_{12}$ (M = Nb and Ta) as obtained from bulk conductivity measurements

Material	Conductivity (S cm^{-1})	Activation energy (eV)	Temperature (°C)	Ref.
$Li_6BaLa_2Nb_2O_{12}$	6.0×10^{-6}	0.44	22	16
$Li_6BaLa_2Nb_2O_{12}$	4.4×10^{-4}	0.35	25	32
$Li_6BaLa_2Ta_2O_{12}$	1.3×10^{-5}	0.44	25	26
$Li_6BaLa_2Ta_2O_{12}$	4.0×10^{-5}	0.40	22	21

Bulk conductivity measurements of garnet-like materials have included the effect of grain boundary resistance and in some cases, different conductivity values for the same materials have been reported.[16,21,26,32] There has also been some disagreement in the literature regarding the activation energy of lithium ion hopping in $Li_6BaLa_2M_2O_{12}$ (M = Ta, Nb). Authors have reported ionic conductivities and activation energies for each of these phases, shown in Table 1. While the more recent studies[26,32] have referred to the previous studies, there is little discussion of the disagreement observed. Differences in the reported values of activation energy for lithium ion hopping likely result from differences in preparation techniques. Typically for bulk conductivity measurements materials are pressed into a pellet and then sintered. Conductivity measurements are taken using inert electrodes.[16] Differences in sintering, pelletizing or general setup could potentially lead to slightly different results. Here, we aim to circumvent some of these issues by using solid-state NMR spectroscopic techniques to consider ionic conductivity in these two phases, as this method can be used to probe local ion dynamics without interference from grain boundary resistance.

1.1. Solid-state ^{6,7}Li NMR of lithium ion electrolytes

^{6,7}Li solid-state NMR is a selective and diagnostic tool to probe ionic motion in lithium ion conductors.[33,34] Differences in the gyromagnetic ratios ($\gamma[^6\text{Li}] : \gamma[^7\text{Li}] = 1 : 2.64$) and natural isotope abundance (^{6}Li = 7.42%, ^{7}Li = 92.58%) allow for a range of different techniques to be used to study structure and dynamics in lithium battery materials. Many cathode materials for lithium ion batteries have been extensively studied using a combination of ^{6}Li and ^{7}Li solid-state NMR spectroscopy, with paramagnetic contributions creating well resolved lithium sites in a wide chemical shift range (>1000 ppm).[6,35,36] Conversely, diamagnetic electrolytes for lithium ion batteries have a small

chemical shift range of −5 to +5 ppm, which results in poorly resolved ^{6,7}Li NMR spectral peaks.[37] Since garnet-like electrolyte materials conduct lithium ions within a single crystallographic site many of the techniques used to study dynamics, such as selective inversion experiments, cannot be applied here.[7,10,27,28] Nuclear relaxation and spin alignment studies offer alternative methods to study such systems. However, there are some limitations, including the sensitivity of nuclear relaxation to processes other than dynamics.[38,39] Here, the change in heteronuclear ^{6}Li–^{7}Li dipolar coupling as a function of temperature is used to probe ionic motion in these materials. This method relies on the distance between heteronuclear spin pairs as well as their respective gyromagnetic ratios, making this a selective method to study dynamics in this system.

1.2. Rotational echo double resonance measurements

REDOR NMR spectroscopy is a technique that measures the dipolar coupling between a pair of heteronuclei.[40,41] This rotor synchronized, double-resonance experiment is traditionally used to determine internuclear distances, making use of the fact that dipolar coupling is related to internuclear distance (r), shown in eqn (1).[31,42]

$$D_{IS} = \hbar\left(\frac{\mu_0}{4\pi}\right)\frac{1}{r_{IS}{}^3}\gamma_i\gamma_j \quad (1)$$

Fig. S1 (ESI†) shows the $I\{S\}$-REDOR NMR pulse sequence. Spin I is observed, while spin S is perturbed as a function of the rotor period. The dipolar coupling between the spin pair allows I to be affected by the perturbation of the S spin. This is examined through the creation of a REDOR curve, which shows the extent of the perturbation as a function of time as the number of pulses on the S spins is increased. The REDOR curve is plotted as $(\Delta S/S_0)$ *vs.* the dephasing time. In this case S_0 is the intensity of a reference Hahn-echo experiment measuring the observed I spectrum, and ΔS is difference between the intensity observed in S_0 and that of the corresponding experiment in which there is a dephasing pulse on the S channel. The term S uses the traditional convention representing the non-observed spin and is not directly related to the term $[\Delta S/S_0]$. The dephasing time is the time allowed for the application of the dephasing pulses on the S channel.

The geometry of the spin pairs in a system is an important factor, which affects the outcome of the REDOR experiment. Many REDOR studies of biological materials take advantage of isotopic labeling to ensure that an isolated pair of nuclei creates a single strong dipolar coupling that can be directly measured in a highly selective, readily quantifiable fashion.[43–46] However, the relationship between ^{6}Li and ^{7}Li in solid-state electrolyte materials is more complex, as the control over the enrichment and isolation of single spin pairs in the structure is not possible. Rather, in these materials there are many ^{6}Li and ^{7}Li spin pairs of varying proximity and the multiple-spin effect must be carefully considered.[47–50] In a system in which there are several spin pairs, a single dipolar coupling between an isolated pair of nuclei is insufficient to describe the system. In this case, each contributing spin pair must be considered if a full quantitative model of the spin system is to be evaluated. For the combination of partial occupancies, and a very large unit cell, this is intractable, and we have focused here on other methods of comparing the dipolar coupling strength in the electrolytes as a function of temperature. These include the use of dipolar second moment, M_2, calculations, and relative scaling of the dipolar curves.

The dipolar second moment is a parameter derived from the summation of all relevant dipolar coupled spin pairs (eqn (3)) and can be used instead of discrete dipolar couplings to fit Spin-Echo Double Resonance (SEDOR) and REDOR curves (eqn (2)).[47] Previous studies have effectively used the analysis of the M_2 to describe the results of stationary ^{6}Li$\{^{7}$Li$\}$-SEDOR experiments aimed to study the spatial distribution of lithium ions in the solid electrolyte glasses $(Li_2O)_x(SiO_2)_{1-x}$ and $(Li_2O)_x(B_2O_3)_{1-x}$.[48,51,52] For prediction of the SEDOR curves each of the heteronuclear spin pairs were included in the calculation of M_2 (eqn (3)) and the experiments performed were able to differentiate between the distributions of cations in these two systems. This type of analysis is also valid for REDOR experiments, which make use of magic angle spinning (MAS) to re-focus the heteronuclear dipolar coupling. This method neglects the effect of homonuclear dipolar coupling, as it is usually removed by MAS.[48]

For systems in which there is a distribution in spin geometries, eqn (1) and (2) can be used to simulate the REDOR curve in the short-term limit, where the REDOR curve is geometry-independent.[47,48] In general this is true for the case in which the term $([S_0 - S]/S_0)$ is $\sim$0.3.[47] In the context of this work, since the REDOR curves (shown in the Results and discussion section) are linear until a dephasing time of 0.005 s, this period will be considered the short-term limit, and the slope of the resulting REDOR curves will be considered geometry-independent.

$$\frac{\Delta S}{S_0} = \frac{4}{3\pi^2}(NT_r)^2 M_2 \quad (2)$$

$$M_2^{\text{hetero}} = \frac{4}{15}\left(\frac{\mu_0}{4\pi}\right)^2 \gamma_I{}^2\gamma_S{}^2\hbar^2 S(S+1)\sum_S r_{IS}{}^{-6} \quad (3)$$

$(\Delta S/S_0)$, defined earlier, is the intensity of the REDOR curve, N is the number of rotor periods, T_r is the length of a single rotor period, and M_2 is the second moment. In eqn (3) the term S is the spin number for the non-observe spin. If M_2 is treated as a variable in eqn (2) the experimental curve can be simulated with a parabola as a function of NT_r with no prior knowledge of the spin geometry. In this case, M_2 can be determined after simulation of the REDOR curve. This method is useful for situations in which there is disorder resulting in local distributions of spins. General limitations to this method include situations in which there is a significant contribution from homonuclear dipolar coupling in which the I–I chemical shifts are different; this may affect the slope or shape of the REDOR curve. Quadrupolar coupling may also contribute to the shape of the REDOR curve. This is particularly relevant for cases in which satellite transitions are present in the non-observed spin, S, and there is concern regarding their contribution to REDOR experiment. ^{7}Li is a prime

example as it tends to have a small quadrupolar coupling that can impact the results of the REDOR experiment.[47]

In the previous work performed by Koller *et al.* (discussed earlier) there was a significant contribution from the quadrupolar nature of ^{11}B, ^{23}Na and ^{27}Al. The authors proposed two different equations for the REDOR curve simulated using M_2 analysis:[30]

$$\frac{\Delta S}{S_0} = \frac{1}{\pi^2 S(S+1)}(N_c T_r)^2 M_2 \quad (4)$$

$$\frac{\Delta S}{S_0} = \frac{5}{\pi^2 S(S+1)}(N_c T_r)^2 M_2 \quad (5)$$

Eqn (4) describes the REDOR curve for a spin-1/2 system, and is equivalent to eqn (2), when S = 1/2. Eqn (5) describes the REDOR curve for a system in which the non-observe spin, S, has a spin of 3/2, and there is excitation of the satellite transitions. The contribution of the quadrupolar interaction to the REDOR curve has been identified previously, however it is usually not quantitatively considered in the interpretation of REDOR data.[30,48]

The REDOR curve is dependent not only on the internuclear distance of a single pair of heteronuclei, but also on the dilution of the ^{6}Li and ^{7}Li in the sample. Li-containing materials can be synthesized using differing amounts of ^{6}Li and ^{7}Li precursors to optimize the heteronuclear dipolar coupling felt by the observed nucleus as well as the signal to noise ratio. The primary focus of our work is the effect of dynamics on ^{6}Li–^{7}Li dipolar coupling and thus on the REDOR curve, since dynamic processes between a pair of nuclei affect the dipolar coupling between them.[8,49,53] Here, we have studied the change in the slopes of the ^{6}Li{^{7}Li}-REDOR curve of the electrolyte materials, $Li_6BaLa_2Ta_2O_{12}$ and $Li_6BaLa_2Nb_2O_{12}$, as a function of temperature to determine the difference in ion mobility between the two samples over the temperature range of 247 K to 350 K. After a series of trials with different isotopic enrichments, the materials were found to be ideal with an isotopic ratio of ~50% ^{6}Li, which gave the optimal results with respect to the sensitivity of the initial slope of the REDOR curve to changes in experimental conditions.

2.0. Experimental

2.1. Synthesis of lithium ion electrolyte materials: $Li_6BaLa_2M_2O_{12}$ (M = Ta, Nb)

High temperature solid-state synthesis methods were used to prepare $Li_6BaLa_2Ta_2O_{12}$ and $Li_6BaLa_2Nb_2O_{12}$. In each case powder X-ray diffraction was used for phase confirmation, shown in the ESI,† Fig. S2.

$Li_6BaLa_2Ta_2O_{12}$. Stoichiometric quantities of La_2O_3 (Aldrich, 99.9%), $Ba(NO_3)_2$ (Aesar, 99+%), Ta_2O_5 (Aldrich, 99%), ^{6}LiOH·H_2O (synthesized from ^{6}Li metal), and LiOH·H_2O (Anachemia, 98%) were ground by hand and placed in a tube furnace (in air) for 12 hours at 700 °C, with heating and cooling ramps of 6 hours each. The mixture was removed, ground again and pelletized. The pellet was sintered in a tube furnace at 900 °C for 24 hours, with a heating and cooling ramp of 12 hours each.

$Li_6BaLa_2Nb_2O_{12}$. The synthesis outlined above was followed, using Nb_2O_5 (Aldrich, 99.99%) in place of Ta_2O_5.

2.2. ^{6,7}Li solid-state NMR

NMR studies were performed on a Bruker Avance I 500 NMR spectrometer. A Bruker 2.5 mm solid-state triple-resonance probe was used with a MAS rate of 30 kHz. Pulse calibration was performed on a 1 M solution of ^{6,7}LiCl (~50% ^{6}Li enriched). For ^{6}Li a nutation frequency of 54 kHz was applied, while for ^{7}Li, a nutation frequency of 88 kHz was applied.

^{6}Li{^{7}Li}-REDOR experiments were performed with a sweep width of 50 ppm, with between 32 and 54 transients collected in the indirect dimension. In the direct dimension, between 32 and 64 transients were co-added, depending on the sample sensitivity. The 180° dephasing pulses on ^{7}Li were equivalent to those calibrated on the 1 M solution of LiCl. Temperatures were calibrated using an external chemical thermometer, $Sm_2Sn_2O_7$.[54]

1D ^{6}Li spectra were collected with a MAS of 30 kHz. For each spectrum the sample was allowed to relax for >2700 s before one single-pulse experiment was performed. Only a single transient was collected in each case to ensure that the correct integration was observed for each lithium site.

1D ^{7}Li spectra were collected with no MAS and also with MAS of 5 kHz. 64 transients were collected with a recycle delay of 60 s.

2.3. Numerical simulations of ^{6}Li{^{7}Li}-REDOR curves

SPINEVOLUTION 3.4.4 software was used to model the ^{6}Li{^{7}Li}-REDOR curve of $Li_6BaLa_2Ta_2O_{12}$ at a low temperature (285 K), where lithium dynamics were found not to contribute to the shapes of the REDOR curves (*vide infra*). Here, we call this the immobile system, since the motion of the lithium ions is slowed to the point at which their motion no longer contributes to the dipolar coupling between pairs of lithium ions.[8] Within the SPINEVOLUTION manual the REDOR experiment is outlined.[55] This was adjusted to include the specific details of the experiment, such as MAS rate, pulse program and the nuclei of interest and is shown in the ESI.† Simulations included a single value for the dipolar coupling. Here we call this the effective dipolar coupling, D_{eff}, and it encompasses all effects contributing to the REDOR curve.

^{6}Li{^{7}Li} heteronuclear second moments were estimated for the Ta and Nb phases according to the following procedure. The 1D ^{6}Li NMR spectra (Fig. 1(b)) were deconvoluted to give the relative peaks areas for the Li-1 and Li-2 sites. The Li-1 and Li-2 site occupancies were then determined from these ratios and the assumption that the number of Li in the chemical formulae was 6 (to maintain charge neutrality), along with the Wyckoff position multiplicity for each site. A disordered structural model was then constructed consisting of a central unit cell and its 26 adjacent unit cells where the Li-1 and Li-2 sites were occupied in a probabilistic manner consistent with their calculated site occupancies. An examination of the crystal structure reveals that the octahedral Li-2 sites occur in symmetry-related pairs separated by only 0.7 Å.[26] Therefore, the structure models did not allow both Li-2 sites in such pairs

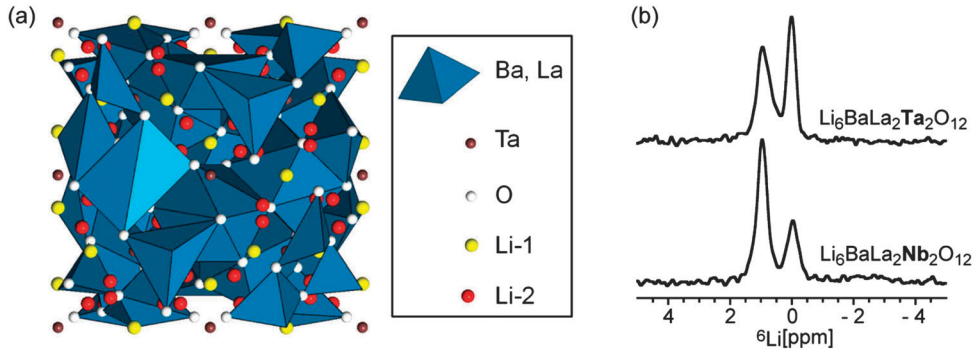

Fig. 1 (a) Illustrated crystal structure of $Li_6BaLa_2Ta_2O_{12}$. The blue polyhedra represent La and Ba, which share a crystallographic site. The brown spheres represent Ta, and the white spheres represent oxygen; while the yellow and red spheres represent Li-1 (tetrahedral) and Li-2 (octahedral), respectively.[26] The image was created in XtalDraw software.[56] (b) ^{6}Li MAS NMR spectrum of $Li_6BaLa_2Ta_2O_{12}$ with MAS 30 kHz. Recycle delays were >2700 s and therefore the tetrahedral site at 0 ppm is thought to be fully relaxed.

to be occupied as this would be physically unreasonable. Also, an examination of the crystal structure reveals that each Li-2 site has two Li-1 sites at distances of 1.74 and 2.31 Å. Since the Li–Li distance of 1.74 Å is quite short, when a Li atom was being placed in one of the Li-2 sites within a pair of close symmetry-related sites, the position furthest away from an occupied Li-1 site was chosen if possible.

Once a disordered structural model was constructed, the various Li atoms were assigned to be ^{6}Li or ^{7}Li in a probabilistic manner consistent with the level of ^{6}Li enrichment (51.45% ^{6}Li). Each ^{6}Li nuclei located in a Li-2 site of the central unit cell was then identified and the distances to ^{7}Li nuclei within 12 Å were calculated (either ^{7}Li nuclei in all Li-1 and Li-2 sites or ^{7}Li nuclei in only Li-2 sites). The second moments were then calculated according to eqn (3) and averaged. This procedure was repeated for 10 000 different disordered structural models and the calculated second moments were averaged again. This procedure was implemented as a *Mathematica* notebook.

3.0. Results and discussion

Solid-state electrolytes $Li_6BaLa_2Ta_2O_{12}$ and $Li_6BaLa_2Nb_2O_{12}$ are known to exhibit stability against attack by commonly used electrode materials, as well as lithium metal. This property makes these materials promising for use in lithium ion batteries. In order to assess these materials before placing them into the battery it is important to understand the mechanism of lithium ion conductivity and the effect of temperature on these materials. Here, solid-state ^{6}Li{^{7}Li}-REDOR NMR has been used to compare these two materials by observing the effect of changing temperature on the distance-dependent ^{6}Li–^{7}Li dipolar coupling.

$^{6,7}Li_6BaLa_2Ta_2O_{12}$ and the corresponding niobium phase were synthesized using high temperature solid-state synthesis methods.[16] The X-ray diffraction patterns of the products showed single-phase, high-purity products, and are in agreement with those reported in the literature, as shown in Fig. S2 in the ESI.† [14] Fig. 1(a) shows the unit cell of $Li_6BaLa_2Ta_2O_{12}$. These materials are known to have two crystallographic lithium sites, with each having a partial occupancy.[26] Cussen *et al.* have studied a related phase $Li_5La_3Ta_2O_{12}$, using neutron diffraction. This phase was shown to crystallize in the same space group of $Ia\bar{3}d$, and reported to have three crystallographic Li sites,[18] confirming the possibility of multiple Li sites within the same phase for these garnet structures.[18] The high quality, high resolution ^{6}Li MAS NMR spectra performed in this work shown in Fig. 1(b) easily confirm that there are two sites: Li-1 and Li-2, which have chemical shifts of 0 and 1 ppm, respectively. Deconvolution in TopSpin 2.1 software reveal the Li contribution of Li-1 and Li-2 to be 41 ± 5% and 58 ± 5%, respectively for the Ta phase; while for the Nb phase the contribution of the Li-1 and Li-2 sites are 25 ± 5% and 75 ± 5%. This is significantly different from the contribution of the Li-1 and Li-2 sites predicted for the Ta phase in previous studies, 15% and 85%, respectively.

T_1 relaxation analysis of these two sites in each phase has shown that the T_1 for the site at 1 ppm is ~12 s, which is at least two orders of magnitude less than the T_1 of the site at 0 ppm. This large difference in T_1 relaxation rate indicates that there is no exchange between the two sites; and also suggests that the site at 1 ppm, with the shorter T_1, is responsible for ion motion.[57] Ionic conductivity in these materials occurs through vacancy-mediated hopping of Li^+ ions, but it is not known to what extent the presence of vacancies affects the rate of ion hopping. Table 2 shows a comparison of the cell constants of the Ta and Nb phases. In this work, as in others, Li-1 has been assigned as the tetrahedral site at 0 ppm, while Li-2 is the octahedral site at 1 ppm and is responsible for lithium ion motion.[26,27]

The relationship between nuclear distance separation and dipolar coupling is well established.[31] Furthermore, the relationship between several heteronuclear spins and their respective separations has been thoroughly described using the dipolar second moment, which is used to analyze experimentally determined REDOR curves.[48,58,59] For the electrolyte materials $Li_6BaLa_2M_2O_{12}$ (M = Ta, Nb) there are four effects which influence the shape of the ^{6}Li{^{7}Li}-REDOR curves obtained:[49]

(1) Distances between ^{6}Li and ^{7}Li spins.[42]

(2) Distribution: site occupancy and resulting dilution of ^{6}Li and ^{7}Li isotopes (affects Li–Li distances); ^{6}Li/^{7}Li isotope ratio;[48] geometry of lithium pairs.

Table 2 $Li_6BaLa_2M_2O_{12}$ cell parameters and calculated values of M_2

	$Li_6BaLa_2Ta_2O_{12}$ (ref. 26)	$Li_6BaLa_2Nb_2O_{12}$ (ref. 16)
Space group	$Ia\bar{3}d$	$Ia\bar{3}d$
Cell constant (Å)	13.001	12.868
Cell volume (Å^3)	2197.51	2130.75
Li-1, Li-2 Wyckoff positions	24*d*, 96*h*	24*d*, 96*h*
^{6}Li NMR peak area ratio	Li-1: 41 ± 5%	Li-1: 25 ± 5%
	Li-2: 58 ± 5%	Li-2: 75 ± 5%
Li-1, Li-2 site occupancies	0.830, 0.293	0.494, 0.377
^{6}Li{^{7}Li} second moment (rad^2 s^{-2})		
^{7}Li in Li-1 and Li-2 sites	2.7×10^7	1.2×10^7
^{7}Li in Li-2 sites only	6.3×10^6	7.8×10^6

(3) Dynamics: the hopping rate between crystallographic lithium sites.[53]

(4) Quadrupolar coupling constant of the non-observe *I* spins, in this case ^{7}Li.[30]

While the distances between crystallographic lithium sites can be determined using X-ray diffraction techniques, the lithium ^{6}Li/^{7}Li isotope dilution and any existing partial occupancies make the construction of a model difficult. The materials studied in this work have less than 50% occupancy of each lithium site.[26]

The changes in the slopes of the ^{6}Li{^{7}Li}-REDOR curves of 50% ^{6}Li enriched $Li_6BaLa_2M_2O_{12}$ (M = Ta, Nb) have been studied in order to qualitatively compare lithium ion hopping rates between these two samples over the same temperature range. This was achieved by comparing the slopes of the experimentally observed REDOR curves of the octahedral site, Li-2 at 1 ppm, at different temperatures. The site resolution in the ^{6}Li spectrum, Fig. 1(b), allows the separation of the REDOR effect for the two sites. The examination of the REDOR curve of samples where the lithium is immobile with respect to the dipolar coupling is an essential piece of the analysis, since it allows the determination of the range of temperatures where the slope is sensitive to changes in temperature.

3.1. Simulation of the immobile ^{6}Li{^{7}Li}-REDOR curve

Second moment calculations as well as numerical simulations for an isolated ^{6}Li/^{7}Li spin pair were used to fit the REDOR curve for the immobile material. This immobile state is achieved by cooling the sample to the point at which only structural characteristics, *i.e.* distances and distribution of the lithium ions, contribute to the slope of the REDOR curve, and is determined experimentally by decreasing the sample temperature and observing the temperature at which there is no more visible change in the REDOR curve. This point marks the point at which the time-scale of dynamics is much slower than the dipolar coupling between the observed ^{6}Li and the surrounding ^{7}Li. In order to observe a change in the slope of the REDOR curve as a function of temperature the time-scale of the ionic hopping rate must correspond to the dipolar coupling in this system.

This immobile state was used as a starting point for comparing the REDOR curves at higher temperatures, since at this point the shape of the curve was determined by the positions of the lithium ions alone, with no contribution from dynamics. Fig. 2 shows the ^{6}Li{^{7}Li}-REDOR curve of $Li_6BaLa_2Ta_2O_{12}$ at 247 K and 285 K.

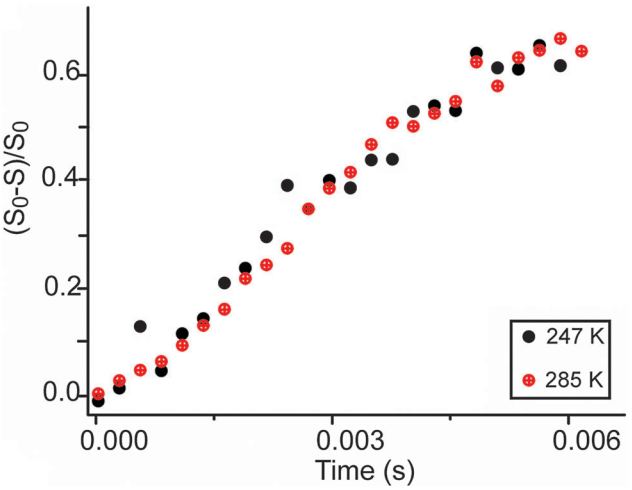

Fig. 2 ^{6}Li{^{7}Li}-REDOR of $^{6,7}Li_6BaLa_2Ta_2O_{12}$ at 247 K and 285 K. The stability in the slope of the REDOR curve indicates that the lithium ions are immobile with respect to the sensitivity of the REDOR experiment. The only influence on this curve is therefore the stationary crystallographic positions of the lithium ions in the material.

The unchanging slope indicates that at these low temperatures, changes in the hopping rate are no longer detectable by this method and the lithium ions are said to be immobile.

Fig. 3 shows efforts to use SPINEVOLUTION software to assess the observed ^{6}Li{^{7}Li}-REDOR curves for the immobile Ta phase using a single ^{6}Li–^{7}Li spin pair.[47,55] Although this is a reasonable fit, this is not an accurate representation of the spin system, which consists of many spin pairs. An attempt to re-construct this system in SPINEVOLUTION software was not successful, since the number of spin pairs is too large. The resulting dipolar coupling is called the effective dipolar coupling, D_{eff}, and is a single value that encompasses the dipolar coupling felt by the ^{6}Li nuclei for all relevant spin pairs. This value can be compared to the dipolar coupling of a single

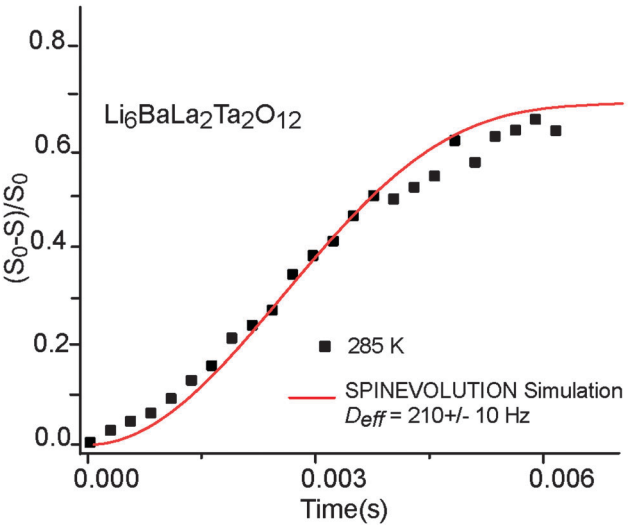

Fig. 3 Analysis of the ^{6}Li{^{7}Li}-REDOR curve of $Li_6BaLa_2Ta_2O_{12}$ using a simulation of ^{6}Li{^{7}Li}-REDOR in SPINEVOLUTION.

pair of ^{7}Li and ^{6}Li nuclei. For comparison, at a distance of 3 Å the dipolar coupling has a value of ~1.6 kHz, which gives a simulated REDOR curve that is much steeper than the one observed in Fig. 2. This is a testament of the effect of the partial occupancy in this system on the experimentally observed REDOR curve.

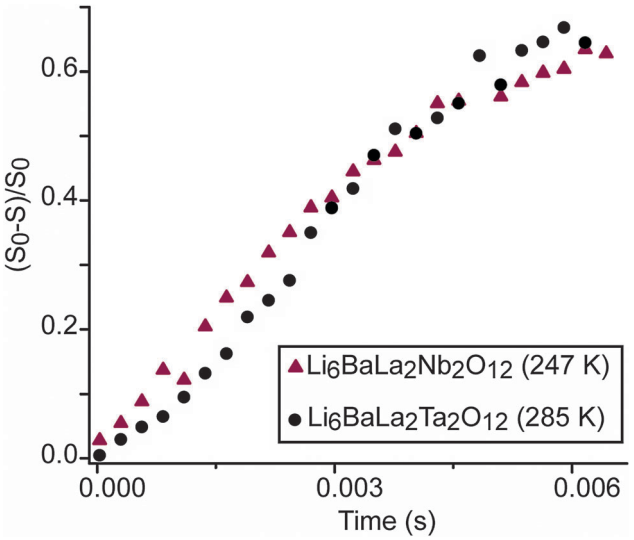

Fig. 4 ^{6}Li{^{7}Li}-REDOR curves of $Li_6BaLa_2M_2O_{12}$ (M = Ta, Nb). In each case the slope represents a point at which dynamics is no longer a contributing factor, and the lithium ions are immobile with respect to the ^{6}Li–^{7}Li dipolar coupling.

3.2. Use of second moment calculations to evaluate structure of Ta and Nb phases

The second moment, M_2, curve was compared to the shape of the ^{6}Li{^{7}Li}-REDOR curves obtained experimentally for the Ta and Nb electrolyte phases. The immobile REDOR curves for these materials are shown in Fig. 4. The general slopes of these curves are very similar, suggesting that the small differences in the unit cells are insufficient to affect the ^{6}Li–^{7}Li dipolar coupling significantly at these low temperatures. However, when the shape of the curve is considered more closely, the initial slopes seem to differ slightly, with the Nb phase having a slightly steeper initial slope.

Second moment calculations for these systems were performed in order to assess the possibility of simulating these curves as a function of temperature. Two models were used to calculate the M_2 values for each material, resulting in a total of four curves shown in Fig. 5(a), along with the experimentally observed curves:

(1) Second moments were calculated with ^{7}Li nuclei in both Li-1 and Li-2 sites, assuming that all ^{7}Li nuclei contribute to dephasing ^{6}Li nuclei in Li-2 sites in the REDOR experiment.

(2) Second moments were calculated with ^{7}Li nuclei in only Li-2 sites, assuming that the ^{7}Li nuclei in the Li-1 sites do not participate in dephasing of ^{6}Li nuclei in Li-2 sites due to their extremely long T_1 relaxation times.

As previously mentioned by Koller *et al.*, there are two equations that could be used, along with the appropriate value of M_2, to simulate the shape the REDOR curve. Eqn (4), shown earlier, describes a case in which the satellite transitions of the non-observed nucleus, in this case ^{7}Li, are not excited by the

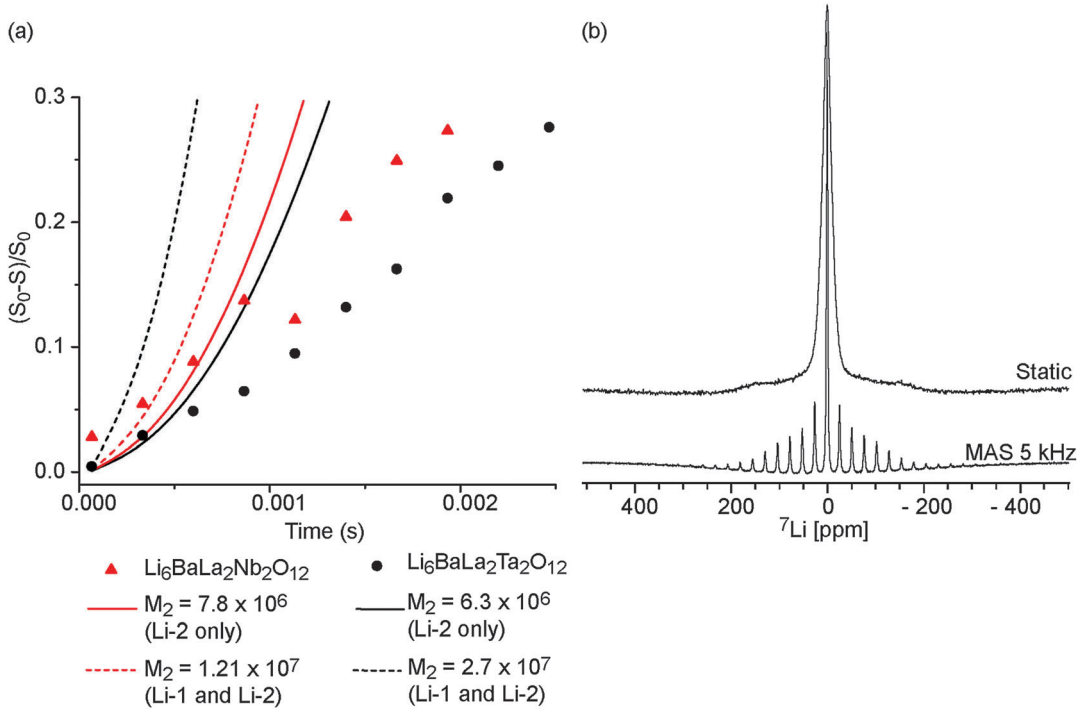

Fig. 5 (a) M_2 calculations for the Ta and Nb electrolyte phases using eqn (4) for cases in which only Li-2 is occupied, and cases in which Li-1 and Li-2 are occupied in the model structure. (b) ^{7}Li NMR spectra of $Li_6BaLa_2Ta_2O_{12}$ with MAS 5 kHz (bottom) and static (top).

NMR experiment. Eqn (5) describes a case in which the satellite transitions are excited in the NMR experiment.

From the static NMR spectrum of $Li_6BaLa_2Ta_2O_{12}$ two satellite transitions from the (+1/2 → +3/2) and (−3/2 → −1/2) transitions can be seen in addition to the central transition (−1/2 → +1/2). These appear as shoulders at approximately +150 ppm and −150 ppm in Fig. 5(b). It is not obvious at the outset whether these satellites contribute to the shape of the observed REDOR curves. However, when M_2 analysis was performed, it was found that the curves that resulted from eqn (4) created a better fit than those of eqn (5), which would suggest that the satellite transition of ^{7}Li did not have a significant effect on the REDOR experiment. As a comparison, simulations using eqn (5) were performed and are shown in Fig. S3 (ESI†). This figure clearly shows that simulations which include the effects of the satellite transitions produce much steeper curves than those observed experimentally and are not in agreement with the experimental data. This indicates that there is no effect from the satellite transitions on the experimentally observed REDOR curves.

An interesting observation from the M_2 calculations was the difference in the simulated curves for the case in which Li-2 was occupied alone and the case in which both Li-1 and Li-2 were occupied. Experimentally, the ^{6}Li{^{7}Li}-REDOR curves look similar, except that the shape is slightly different for the initial lower values of ($[S_0 - S]/S_0$) on the curve. In this range it would seem that the REDOR curve of the Ta phase has a *more shallow* slope than that of the Nb phase. On performing the M_2 analysis, the opposite trend was observed for the model in which both Li-1 and Li-2 sites were occupied, dashed lines in Fig. 5(a). The M_2 calculations in this case suggest that the slope of the Ta REDOR curve is *larger* than that of the Nb phase. Conversely, when the M_2 analysis is performed and only Li-2 is occupied the order is reversed and the calculations reveal that the slope of the Nb REDOR curve is *larger* than that of the Ta curve. This latter trend is in agreement with the experimental data and is represented by the solid lines in Fig. 5(a). The reason for this agreement is thought to be that the lithium in the Li-1 site does not contribute to the REDOR curves in reality due to the long T_1 relaxation of this site.

Overall, the M_2 simulations exhibit a modest representation of the experimentally observed REDOR curves, however, the curves appear to be in the expected range. Differences between calculated M_2 curves and experimental REDOR curves can be attributed to the contribution from the quadrupole coupling of both ^{6}Li and ^{7}Li, homonuclear dipolar coupling, as well as any disorder in the structure. There could also be residual ''rattling'' motions within the cages of the octahedral site, where lithium ions vibrate within the octahedral environment. This effect is not temperature dependent, but could contribute to the dipolar coupling between Li pairs, and has been observed previously in ^{7}Li{^{31}P}-REDOR studies of $Li_3V_2(PO_4)_3$.[8]

3.3. Examining dynamics using the initial slope of the ^{6}Li{^{7}Li}-REDOR curve of $^{6,7}Li_6BaLa_2Ta_2O_{12}$

Here, we have made use of the slope of the initial ^{6}Li{^{7}Li}-REDOR curve of $Li_6BaLa_2Ta_2O_{12}$ for a 50% ^{6}Li enriched sample to describe changes as a function of temperature to indicate the temperature dependence of the lithium ion hopping rate. The initial slope of the REDOR curve has been shown to be independent of sample geometry, *i.e.* the relative orientation of lithium ions. Studies of $Li_6BaLa_2Ta_2O_{12}$ show that the REDOR slope is sensitive to changes in temperature and this temperature dependence can be correlated to changes in dynamics in the system. Fig. 6 shows the effect of temperature on the REDOR curve of $Li_6BaLa_2Ta_2O_{12}$. Increasing the temperature from 285 K, where the ions are immobile, to 350 K produces a steady decrease in the slope of the REDOR curve, which is indicative of an increase in the rate of ionic motion within this temperature range, and causes an apparent decrease in the dipolar coupling.

Fig. 7 shows the temperature dependent REDOR curves along with the respective slopes, P, which begin at a value of $123 \pm 2\ s^{-1}$ for the immobile REDOR curve and decreases as the temperature increases. The temperature dependent slopes are summarized in Table 3. Here, P changes from $123 \pm 2\ s^{-1}$ to $66 \pm 1\ s^{-1}$ over a temperature range of 285 K to 350 K. Values of P can also be used to compare ionic mobility in similar samples where the Li–Li separation is the same and the only factor affecting the change in the slope of the REDOR curve is a change in ion hopping rate. Here, the slope of the immobile curve is unchanging below 285 K.

3.4. ^{6}Li{^{7}Li}-REDOR of $^{6,7}Li_6BaLa_2Nb_2O_{12}$

Ion mobility in different materials can be directly compared using ^{6}Li{^{7}Li}-REDOR provided the materials are similar in structure (lithium content, framework structure and Li–Li internuclear distances). A prime use of this method is the comparison of two crystalline materials, which differ only in framework atoms, such as $Li_6BaLa_2Ta_2O_{12}$ and $Li_6BaLa_2Nb_2O_{12}$, where Ta and Nb occupy the same crystallographic sites within in their respective materials. Thus, changes in the slopes of the REDOR curves are attributed to differences in temperature dependent lithium ion dynamics alone. Minor differences in the shapes of the REDOR curves, shown in Fig. 4, for these two samples can be

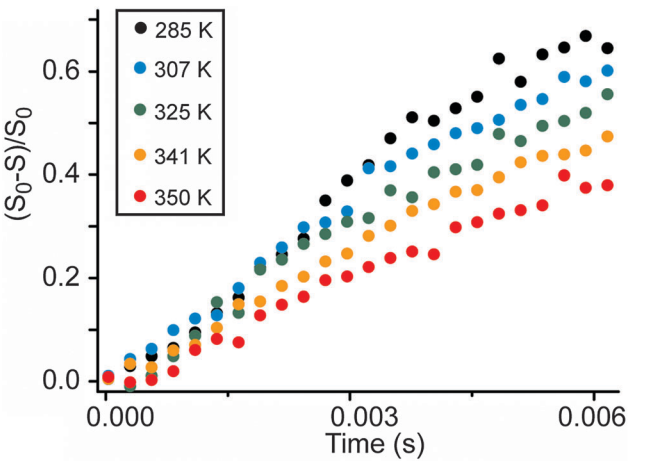

Fig. 6 Variable temperature ^{6}Li{^{7}Li}-REDOR curves of 50% ^{6}Li enriched $Li_6BaLa_2Ta_2O_{12}$. Increasing temperature causes a decrease in the slope of the REDOR curve.

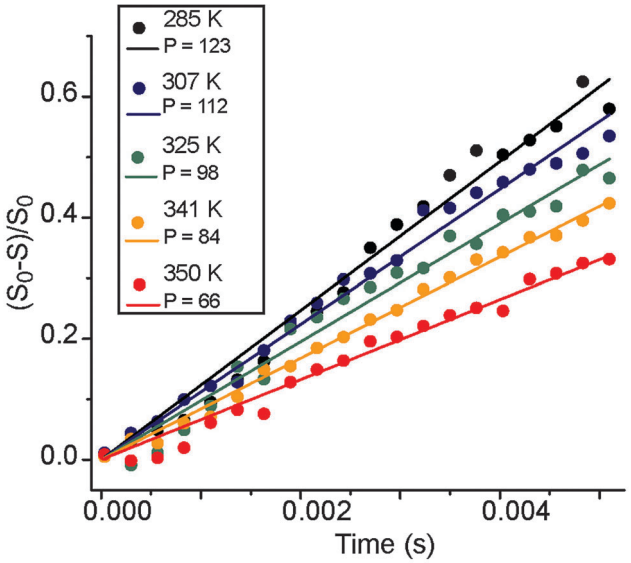

Fig. 7 Initial slopes, P, of the ^{6}Li{^{7}Li}-REDOR curves of $Li_6BaLa_2Ta_2O_{12}$ as a function of temperature. Solid circles represent the experimentally obtained REDOR curves, as in Fig. 6; while the solid lines represent the lines of best fit. Over the temperature range of 285 K, where the dynamics processes are static, to 350 K P ranges from 123 ± 2 s^{-1} to 66 ± 1 s^{-1}.

Table 3 Temperature dependent slopes of ^{6}Li{^{7}Li}-REDOR curves of $Li_6BaLa_2Ta_2O_{12}$ and $Li_6BaLa_2Nb_2O_{12}$

Temperature (K)	P (s^{-1}) $Li_6BaLa_2Ta_2O_{12}$	Temperature (K)	P (s^{-1}) $Li_6BaLa_2Nb_2O_{12}$
285	123 ± 2	247	140 ± 10
307	112 ± 2	273	76 ± 3
325	98 ± 2	294	33 ± 2
341	84 ± 2	312	26 ± 2
350	66 ± 1	325	19 ± 1
		332	12 ± 1
		341	10.2 ± 0.5
		350	8.3 ± 0.5

attributed to differences in the distribution of lithium ions in these structures. In Fig. 1 the ^{6}Li MAS NMR spectra show that although the absolute lithium ion content is the same, there is some variation in the lithium ion occupancy between the two sites in the Nb and Ta phases. It seems that the Nb phase has a higher content of Li ions in the octahedral environments, Li-2.

To directly compare the lithium dynamics in this system, the variable temperature ^{6}Li{^{7}Li}-REDOR curves of $Li_6BaLa_2M_2O_{12}$ (M = Ta, Nb) have been considered. Fig. 8 shows the ^{6}Li{^{7}Li}-REDOR curves for the Nb material obtained over the temperature range of 247 K to 350 K. With increasing temperature the slopes of the REDOR curves change dramatically, particularly at higher temperatures. The temperature dependent slopes are summarized in Table 3. On considering the behaviour of P, it is evident that there is a much more significant contribution from dynamics in the Nb material than for the Ta material. The Nb phase exhibits a slope of 8.3 ± 0.5 s^{-1} at 350 K, while the Ta phase has a slope of only 66 ± 1 s^{-1} at the same temperature as shown in Fig. 7.

With such different variations in the slopes over the same temperature range it is clear that the ionic motion in the Ta and Nb phases is quite different. While the literature predicts that these materials have differences in ionic conductivity and activation energy, it is unclear to what extent, since this is a point of disagreement. The most recent study of $Li_6BaLa_2Nb_2O_{12}$ reports an ionic conductivity of 4.4 × 10^{-4} S cm^{-1} with an activation energy of 0.35 eV.[32] While the most recent study of the Ta phase reports an ionic conductivity of 1.3 × 10^{-5} S cm^{-1} and an activation energy of 0.44 eV.[26] Their result would indicate that the Nb phase is an overall better material when considering ionic conductivity and activation energy. The results obtained in this study indicate qualitatively that the Nb phase has an overall higher ionic conductivity at room temperature than the Ta phase due to the smaller value of the slope, P, at room temperature.

NMR spectroscopy is capable of observing ionic motion within the particle, and therefore grain boundary resistance does not play a role in the measurement of ion hopping processes, whereas in bulk conductivity measurements, it is difficult to remove the inherent bulk effects. The NMR spectroscopic data collected here shows that the Nb phase is clearly the better ionic conductor, while previous bulk conductivity measurements have been inconclusive.

A pseudo-Arrhenius analysis of the changes in P for $Li_6BaLa_2M_2O_{12}$ (M = Ta, Nb) was performed and is shown in Fig. 9. This plot shows that the changes in the slopes of the REDOR curves follow a consistent trend. The slopes of the pseudo-Arrhenius plots are clearly different for the Ta and Nb phases. The Ta phase has a slope of 1.2 ± 0.2 K, while the Nb phase has a steeper slope of 2.7 ± 0.1 K. This indicates that there is likely a difference in the activation energy of local lithium ion hopping in these materials within this temperature range, with the larger activation energy of the Nb-phase being attributed to its slightly smaller unit cell size. For this analysis, the data points that correspond to the REDOR curves with the lowest temperatures are not considered. The low temperature measurements were taken to determine the specific temperature (freezing point) at which the slope was no longer temperature dependent, and thus the slopes corresponding to the lowest temperatures represent a point of convergence of the slopes at low temperature.

This study is capable of qualitatively determining which of these materials shows a greater response to changes in temperature, and thereby indicates which phase is a better ion conductor at a particular temperature. However, the results do not lead to straightforward quantitative conductivity data since the relationship between the changes in P and changes in ionic hopping rate are not precisely defined from this method. $Li_6BaLa_2Nb_2O_{12}$ appears to have higher ionic conductivity at room temperature. Although the Ta and Nb structures appear to be very similar, it is likely that the difference in the distribution of lithium ions within each structure contributes to differences in ion mobility.

The ^{6}Li MAS NMR spectra in Fig. 1(b) show that there is a greater ratio of lithium in the octahedral site in each of the Ta and Nb phases studied here. This site, Li-2, is known to be

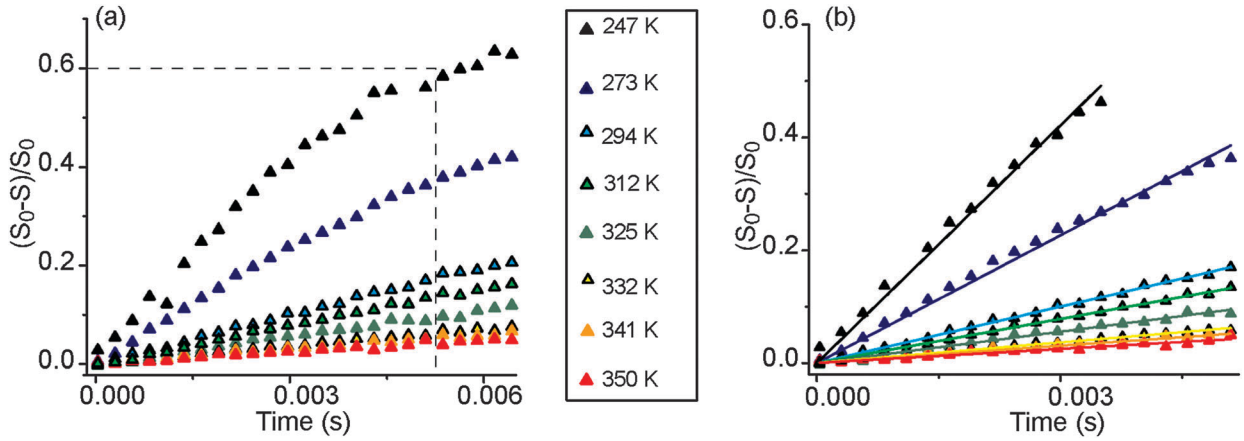

Fig. 8 (a) ^{6}Li{^{7}Li}-REDOR curves of $Li_6BaLa_2Nb_2O_{12}$ over the temperature range of 247 K, where the sample is immobile, to 350 K. (b) Lines of best fit for each temperature have slopes P, which range from 140 ± 10 s^{-1}, for the immobile sample, to 8.3 ± 0.5 s^{-1}.

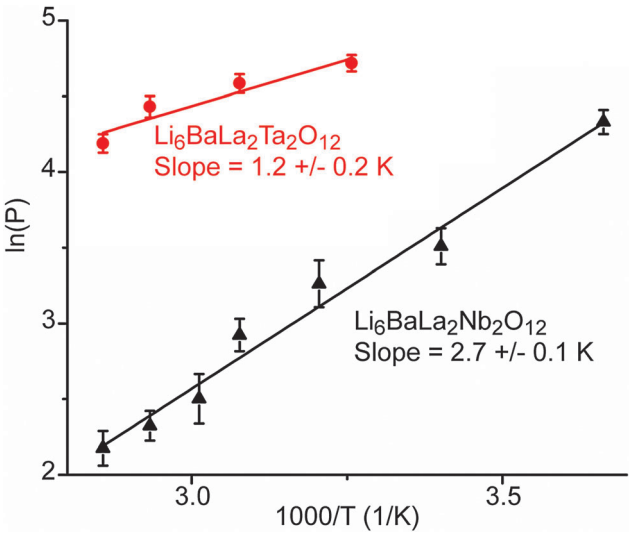

Fig. 9 Pseudo-Arrhenius analysis of P for $Li_6BaLa_2M_2O_{12}$ (M = Ta, Nb). The red circles represent the Ta phase, while the black triangles represent the Nb phase. The slopes are 1.2 ± 0.2 K and 2.7 ± 0.1 K, respectively, for the Ta and Nb phases.

solely responsible for lithium ion motion in these phases. For the Nb phase, there is significantly more Li in the Li-2 site, while the NMR results show that this phase exhibits higher ionic conductivity at room temperature. Together, these findings suggest that the higher content of lithium in Li-2 in the Nb phase may explain the observed higher ionic conductivity in the Nb phase when compared to the Ta counterpart. In previous studies the extent to which the concentration of lithium in a single site contributes to the ion hopping rate was not evident. Whereas, this study demonstrates that a higher population of Li in the octahedral site is correlated with an increase in the rate of Li ion hopping.

While both the absolute conductivity, and the temperature-dependent conductivity of a sample need to be optimized for any actual application, these properties are not directly linked. It is interesting to note that some optimum concentration of Li in the Li-2 site may be found, where the conductivity and activation energy are tuned to specific targets. It is hypothesized that the increased activation energy of the Nb phase could also be the result of the increasing occupancy in the conducting site, causing a knock-on mechanism of ion transport, in the limit of highest site occupancy.

4.0. Conclusion

Solid-state ^{6}Li{^{7}Li}-REDOR NMR spectroscopy has been used to compare the ionic conductivity in $Li_6BaLa_2M_2O_{12}$ (M = Ta, Nb). ^{6}Li{^{7}Li}-REDOR NMR was used to indirectly study changes in ^{6}Li–^{7}Li dipolar coupling as a function of temperature, which were related to the changes in ion mobility by examining the temperature dependence of slope of the resulting REDOR curve. Higher temperatures increased the ionic mobility for each of the phases, resulting in a shallower slope of the REDOR curve. This occurs as a result of increased mobility at a hopping rate similar to the ^{6}Li–^{7}Li dipolar coupling. The curves were characterised according to the slope, P. The Nb phase showed a greater change in P with increasing temperature, and thus generated a steeper slope in the pseudo-Arrhenius analysis. While this method does not quantitatively measure the ionic hopping rate, it clearly points out that the Nb material has higher ion hopping rate than the Ta phase at room temperature and above. In addition it is indicated that the Nb phase has a higher activation energy for lithium ion hopping when compared to the Ta counterpart.

The reason for the observed differences in ion conductivity between these two phases is likely the difference in the lithium ion distribution among the two existing crystallographic sites. ^{6}Li MAS NMR spectra have revealed that the Nb phase has a higher content of lithium in the octahedral environment, which is responsible for lithium ion motion.

Acknowledgements

The authors would like to acknowledge the generous funding for this project provided by the National Sciences and Engineering

Research Council of Canada (NSERC). In addition, we would like to thank Prof. Alex Bain for many stimulating discussions.

References

1 J. B. Goodenough and K. S. Park, The Li-Ion Rechargeable Battery: A Perspective, *J. Am. Chem. Soc.*, 2013, **135**(4), 1167–1176.
2 J. M. Tarascon and M. Armand, Issues and challenges facing rechargeable lithium batteries, *Nature*, 2001, **414**(6861), 359–367.
3 J. B. Goodenough and Y. Kim, Challenges for Rechargeable Li Batteries, *Chem. Mater.*, 2010, **22**(3), 587–603.
4 H. Y. Chen, M. Armand, M. Courty, M. Jiang, C. P. Grey, F. Dolhem, J. M. Tarascon and P. Poizot, Lithium Salt of Tetrahydroxybenzoquinone: Toward the Development of a Sustainable Li-Ion Battery, *J. Am. Chem. Soc.*, 2009, **131**(25), 8984–8988.
5 R. Bhattacharyya, B. Key, H. L. Chen, A. S. Best, A. F. Hollenkamp and C. P. Grey, In situ NMR observation of the formation of metallic lithium microstructures in lithium batteries, *Nat. Mater.*, 2010, **9**(6), 504–510.
6 C. P. Grey and Y. J. Lee, Lithium MAS NMR studies of cathode materials for lithium-ion batteries, *Solid State Sci.*, 2003, **5**(6), 883–894.
7 L. S. Cahill, R. P. Chapman, J. F. Britten and G. R. Goward, Li-7 NMR and two-dimensional exchange study of lithium dynamics in monoclinic $Li_3V_2(PO_4)_3$, *J. Phys. Chem. B*, 2006, **110**(14), 7171–7177.
8 L. S. Cahill, C. W. Kirby and G. R. Goward, Li-6{P-31} rotational-echo, double-resonance studies of lithium ion site dynamics in $Li_3V_2(PO_4)_3$, *J. Phys. Chem. C*, 2008, **112**(6), 2215–2221.
9 L. S. Cahill, S. C. Yin, A. Samoson, I. Heinmaa, L. F. Nazar and G. R. Goward, Li-6 NMR studies of cation disorder and transition metal ordering in $Li[Ni_{1/3}Mn_{1/3}Co_{1/3}]O_2$ using ultrafast magic angle spinning, *Chem. Mater.*, 2005, **17**(26), 6560–6566.
10 L. J. M. Davis, X. J. He, A. D. Bain and G. R. Goward, Studies of lithium ion dynamics in paramagnetic cathode materials using Li-6 1D selective inversion methods, *Solid State Nucl. Magn. Reson.*, 2012, **42**, 26–32.
11 N. Dupre, J. Oliveri, J. Degryse, J. F. Martin and D. Guyomard, Characterization of the surface of positive electrodes for Li-ion batteries using Li-7 MAS NMR, *Ionics*, 2008, **14**(3), 203–207.
12 N. Yamakawa, M. Jiang, B. Key and C. P. Grey, Identifying the Local Structures Formed during Lithiation of the Conversion Material, Iron Fluoride, in a Li Ion Battery: a Solid-State NMR, X-ray Diffraction, and Pair Distribution Function Analysis Study, *J. Am. Chem. Soc.*, 2009, **131**(30), 10525–10536.
13 B. Key, R. Bhattacharyya, M. Morcrette, V. Seznec, J. M. Tarascon and C. P. Grey, Real-Time NMR Investigations of Structural Changes in Silicon Electrodes for Lithium-Ion Batteries, *J. Am. Chem. Soc.*, 2009, **131**(26), 9239–9249.
14 V. Thangadurai and W. Weppner, Investigations on electrical conductivity and chemical compatibility between fast lithium ion conducting garnet-like $Li_6BaLa_2Ta_2O_{12}$ and lithium battery cathodes, *J. Power Sources*, 2005, **142**(1–2), 339–344.
15 V. Thangadurai, J. Schwenzel and W. Weppner, Tailoring ceramics for specific applications: a case study of the development of all-solid-state lithium batteries, *Ionics*, 2005, **11**(1–2), 11–23.
16 V. Thangadurai and W. Weppner, $Li_6ALa_2Nb_2O_{12}$ (A = Ca, Sr, Ba): A new class of fast lithium ion conductors with garnet-like structure, *J. Am. Ceram. Soc.*, 2005, **88**(2), 411–418.
17 M. Nakayama, M. Kotobuki, H. Munakata, M. Nogami and K. Kanamura, First-principles density functional calculation of electrochemical stability of fast Li ion conducting garnet-type oxides, *Phys. Chem. Chem. Phys.*, 2012, **14**(28), 10008–10014.
18 E. J. Cussen, The structure of lithium garnets: cation disorder and clustering in a new family of fast Li^+ conductors, *Chem. Commun.*, 2006, 412–413.
19 J. Awaka, N. Kijima, H. Hayakawa and J. Akimoto, Synthesis and structure analysis of tetragonal $Li_7La_3Zr_2O_{12}$ with the garnet-related type structure, *J. Solid State Chem.*, 2009, **182**(8), 2046–2052.
20 H. Buschmann, J. Dolle, S. Berendts, A. Kuhn, P. Bottke, M. Wilkening, P. Heitjans, A. Senyshyn, H. Ehrenberg, A. Lotnyk, V. Duppel, L. Kienle and J. Janek, Structure and dynamics of the fast lithium ion conductor "$Li_7La_3Zr_2O_{12}$", *Phys. Chem. Chem. Phys.*, 2011, **13**(43), 19378–19392.
21 V. Thangadurai and W. Weppner, $Li_6ALa_2Ta_2O_{12}$ (A = Sr, Ba): novel garnet-like oxides for fast lithium ion conduction, *Adv. Funct. Mater.*, 2005, **15**(1), 107–112.
22 T. Vosegaard, I. P. Byriel, D. A. Pawlak, K. Wozniak and H. J. Jakobsen, Crystal structure studies on the garnet $Y_3Al_5O_{12}$ by Al-27 single-crystal NMR spectroscopy, *J. Am. Chem. Soc.*, 1998, **120**(31), 7900–7904.
23 V. Thangadurai, S. Adams and W. Weppner, Crystal structure revision and identification of Li^+-ion migration pathways in the garnet-like $Li_5La_3M_2O_{12}$ (M = Nb, Ta) oxides, *Chem. Mater.*, 2004, **16**(16), 2998–3006.
24 M. P. O'Callaghan and E. J. Cussen, Lithium dimer formation in the Li-conducting garnets $Li_{5+x}Ba_xLa_{3-x}Ta_2O_{12}$ ($0 < x \leq 1.6$), *Chem. Commun.*, 2007, 2048–2050.
25 R. Murugan, V. Thangadurai and W. Weppner, Fast lithium ion conduction in garnet-type $Li_7La_3Zr_2O_{12}$, *Angew. Chem., Int. Ed.*, 2007, **46**(41), 7778–7781.
26 J. Awaka, N. Kijima, Y. Takahashi, H. Hayakawa and J. Akimoto, Synthesis and crystallographic studies of garnet-related lithium-ion conductors $Li_6CaLa_2Ta_2O_{12}$ and $Li_6BaLa_2Ta_2O_{12}$, *Solid State Ionics*, 2009, **180**(6–8), 602–606.
27 M. P. O'Callaghan, A. S. Powell, J. J. Titman, G. Z. Chen and E. J. Cussen, Switching on fast lithium ion conductivity in garnets: The structure and transport properties of $Li_{3+x}Nd_3Te_{2-x}Sb_xO_{12}$, *Chem. Mater.*, 2008, **20**(6), 2360–2369.
28 L. van Wullen, T. Echelmeyer, H. W. Meyer and D. Wilmer, The mechanism of Li-ion transport in the garnet $Li_5La_3Nb_2O_{12}$, *Phys. Chem. Chem. Phys.*, 2007, **9**(25), 3298–3303.

29 M. Nyman, T. M. Alam, S. K. McIntyre, G. C. Bleier and D. Ingersoll, Alternative Approach to Increasing Li Mobility in Li-La-Nb/Ta Garnet Electrolytes, *Chem. Mater.*, 2010, **22**(19), 5401–5410.
30 H. Koller and M. Kalwei, Studying ionic motion in tetrahydroxoborate sodalite by second moment analysis using Na-23{B-11} rotational echo double resonance data, *J. Phys. Chem. B*, 2004, **108**(1), 58–63.
31 T. Gullion and J. Schaefer, Rotational-Echo Double-Resonance NMR, *J. Magn. Reson.*, 1989, **81**(1), 196–200.
32 L. Truong and V. Thangadurai, Soft-Chemistry of Garnet-Type $Li_{5+x}Ba_xLa_{3-x}Nb_2O_{12}$ (x = 0, 0.5, 1): Reversible $H^+ \leftrightarrow Li^+$ Ion-Exchange Reaction and Their X-ray, Li-7 MAS NMR, IR, and AC Impedance Spectroscopy Characterization, *Chem. Mater.*, 2011, **23**(17), 3970–3977.
33 Y. J. Lee, F. Wang and C. P. Grey, Li-6 and Li-7 MAS NMR studies of lithium manganate cathode materials, *J. Am. Chem. Soc.*, 1998, **120**(48), 12601–12613.
34 M. Klett, M. Giesecke, A. Nyman, F. Hallberg, R. W. Lindstrom, G. Lindbergh and I. Furo, Quantifying Mass Transport during Polarization in a Li Ion Battery Electrolyte by *in situ* Li-7 NMR Imaging, *J. Am. Chem. Soc.*, 2012, **134**(36), 14654–14657.
35 L. S. Cahill, R. P. Chapman, C. W. Kirby and G. R. Goward, The challenge of paramagnetism in two-dimensional Li-6, Li-7 exchange NMR, *Appl. Magn. Reson.*, 2007, **32**(4), 565–581.
36 L. J. M. Davis, I. Heinmaa and G. R. Goward, Study of Lithium Dynamics in Monoclinic $Li_3Fe_2(PO_4)_3$ using Li-6 VT and 2D Exchange MAS NMR Spectroscopy, *Chem. Mater.*, 2010, **22**(3), 769–775.
37 Z. Xu and J. F. Stebbins, Li-6 Nuclear-Magnetic-Resonance Chemical-Shifts, Coordination-Number and Relaxation in Crystalline and Glassy Silicates, *Solid State Nucl. Magn. Reson.*, 1995, **5**(1), 103–112.
38 A. Kuhn, V. Epp, G. Schmidt, S. Narayanan, V. Thangadurai and M. Wilkening, Spin-alignment echo NMR: probing Li^+ hopping motion in the solid electrolyte $Li_7La_3Zr_2O_{12}$ with garnet-type tetragonal structure, *J. Phys.: Condens. Matter*, 2012, **24**(3), 1–8.
39 A. Kuhn, S. Narayanan, L. Spencer, G. Goward, V. Thangadurai and M. Wilkening, Li self-diffusion in garnet-type $Li_7La_3Zr_2O_{12}$ as probed directly by diffusion-induced Li-7 spin-lattice relaxation NMR spectroscopy, *Phys. Rev. B: Condens. Matter Mater. Phys.*, 2010, **83**(9), 094302.
40 C. Fernandez, D. P. Lang, J. P. Amoureux and M. Pruski, Measurement of heteronuclear dipolar interactions between quadrupolar and spin-1/2 nuclei in solids by multiple-quantum REDOR NMR, *J. Am. Chem. Soc.*, 1998, **120**(11), 2672–2673.
41 T. T. Tran, D. Herfort, H. J. Jakobsen and J. Skibsted, Site Preferences of Fluoride Guest Ions in the Calcium Silicate Phases of Portland Cement from Si-29{F-19} CP-REDOR NMR Spectroscopy, *J. Am. Chem. Soc.*, 2009, **131**(40), 14170–14171.
42 T. Gullion, Introduction to rotational-echo, double-resonance NMR, *Concepts Magn. Reson.*, 1998, **10**(5), 277–289.
43 O. Toke, L. Cegelski and J. Schaefer, Peptide antibiotics in action: Investigation of polypeptide chains in insoluble environments by rotational-echo double resonance, *Biochim. Biophys. Acta, Biomembr.*, 2006, **1758**(9), 1314–1329.
44 C. P. Jaroniec, B. A. Tounge, C. M. Rienstra, J. Herzfeld and R. G. Griffin, Measurement of C-13-N-15 distances in uniformly C-13 labeled biomolecules: J-decoupled REDOR, *J. Am. Chem. Soc.*, 1999, **121**(43), 10237–10238.
45 M. E. Merritt, A. M. Christensen, K. J. Kramer, T. L. Hopkins and J. Schaefer, Detection of intercatechol cross-links in insect cuticle by solid-state carbon-13 and nitrogen-15 NMR, *J. Am. Chem. Soc.*, 1996, **118**(45), 11278–11282.
46 M. E. Merritt, S. T. Sigurdsson and G. P. Drobny, Long-range distance measurements to the phosphodiester backbone of solid nucleic acids using P-31-F-19 REDOR NMR, *J. Am. Chem. Soc.*, 1999, **121**(25), 6070–6071.
47 M. Bertmer and H. Eckert, Dephasing of spin echoes by multiple heteronuclear dipolar interactions in rotational echo double resonance NMR experiments, *Solid State Nucl. Magn. Reson.*, 1999, **15**(3), 139–152.
48 S. P. Puls and H. Eckert, Spatial distribution of lithium ions in glasses studied by Li-7{Li-6} spin echo double resonance, *Phys. Chem. Chem. Phys.*, 2007, **9**(30), 3992–3998.
49 J. M. Goetz and J. Schaefer, REDOR dephasing by multiple spins in the presence of molecular motion, *J. Magn. Reson.*, 1997, **127**(2), 147–154.
50 V. R. Celinski, J. Weber and J. S. A. der Gunne, C-REDOR curves of extended spin systems, *Solid State Nucl. Magn. Reson.*, 2013, **49–50**, 12–22.
51 T. M. Alam, J. McLaughlin, C. C. Click, S. Conzone, R. K. Brow, T. J. Boyle and J. W. Zwanziger, Investigation of sodium distribution in phosphate glasses using spin-echo Na-23 NMR, *J. Phys. Chem. B*, 2000, **104**(7), 1464–1472.
52 J. Tsuchida, J. Schneider, R. R. Deshpande and H. Eckert, Cation Distribution and Local Order in Mixed Sodium Metaphosphate Glasses, *J. Phys. Chem. C*, 2012, **116**(46), 24449–24461.
53 S. Dupke, T. Langer, R. Pottgen, M. Winter, S. Passerini and H. Eckert, Structural characterization of the lithium silicides $Li_{15}Si_4$, $Li_{13}Si_4$, and Li_7Si_3 using solid state NMR, *Phys. Chem. Chem. Phys.*, 2012, **14**(18), 6496–6508.
54 C. P. Grey, A. K. Cheetham and C. M. Dobson, Temperature-Dependent Solid-State Sn-119 MAS NMR of $Nd_2Sn_2O_7$, $Sm_2Sn_2O_7$, and $Y_{1.8}Sm_{0.2}Sn_2O_7$ - 3 Sensitive Chemical-Shift Thermometers, *J. Magn. Reson., Ser. A*, 1993, **101**(3), 299–306.
55 M. Veshtort and R. G. Griffin, SPINEVOLUTION: a powerful tool for the simulation of solid and liquid state NMR experiments, *J. Magn. Reson.*, 2006, **178**(2), 248–282.
56 B. Downs and K. B. Kausil Simmaswamy, *XtalDraw*, 2003.
57 D. C. Apperley, R. K. Harris and P. Hodgkinson, *Solid-State NMR: Principles and Practice*, Momentum Press, New York, 2012, p. 276.
58 B. Gee and H. Eckert, Cation distribution in mixed-alkali silicate glasses. NMR studies by Na-23-{Li-7} and Na-23-{Li-6} spin echo double resonance, *J. Phys. Chem.*, 1996, **100**(9), 3705–3712.
59 S. Causemann, M. Schonhoff and H. Eckert, Local environment and distribution of alkali ions in polyelectrolyte complexes studied by solid-state NMR, *Phys. Chem. Chem. Phys.*, 2011, **13**(19), 8967–8976.

